Biomechanical Analysis of the Three-Dimensional Foot Structure During Gait: A Basic Tool for Clinical Applications

A. Gefen
Department of Biomedical Engineering,
Faculty of Engineering,
Tel Aviv University,
Tel Aviv 69978, Israel

M. Megido-Ravid

Y. Itzchak

Department of Diagnostic Imaging,
The H. Sheba Medical Center,
Tel Hashomer 52621, Israel

M. Arcan
Department of Biomedical Engineering,
Faculty of Engineering,
Tel Aviv University,
Tel Aviv 69978, Israel

A novel three-dimensional numerical model of the foot, incorporating, for the first time in the literature, realistic geometric and material properties of both skeletal and soft tissue components of the foot, was developed for biomechanical analysis of its structural behavior during gait. A system of experimental methods, integrating the optical Contact Pressure Display (CPD) method for plantar pressure measurements and a Digital Radiographic Fluoroscopy (DRF) instrument for acquisition of skeletal motion during gait, was also developed in this study and subsequently used to build the foot model and validate its predictions. Using a Finite Element solver, the stress distribution within the foot structure was obtained and regions of elevated stresses for six subphases of the stance (initial-contact, heel-strike, midstance, forefoot-contact, push-off, and toe-off) were located. For each of these subphases, the model was adapted according to the corresponding fluoroscopic data, skeletal dynamics, and active muscle force loading. Validation of the stress state was achieved by comparing model predictions of contact stress distribution with respective CPD measurements. The presently developed measurement and numerical analysis tools open new approaches for clinical applications, from simulation of the development mechanisms of common foot disorders to pre- and post-interventional evaluation of their treatment. [S0148-0731(00)01106-7]

Keywords: *Numerical Modeling, Plantar Pressure, Skeletal Motion, Contact Stress, Stance*

Introduction

The foot structure, a vital connection between the human body and the ground, plays a highly important role in human locomotion. Knowledge of the dynamic stress evolution within and between its different structural components is a key for understanding their respective function during gait, and will also allow a better comprehension of some disorders. Despite the critical role of the foot, quantitative kinematic and dynamic analysis during gait is still in its infancy. The present study is therefore aimed to develop an integrated system of experimental and numerical tools, in order to analyze the three-dimensional foot structural behavior during gait and to open new approaches for clinical applications.

Since direct measurements of the stress distribution within the human foot *in vivo* during gait are not feasible, the use of a model, subjected to dynamic muscle and structural loading, as well as to a set of ground constraints, is the only alternative for carrying out such an investigation. Modeling of the foot necessarily confronts a three-dimensional problem. Stresses within the foot structure are dependent on the three-dimensional geometry of its components (hard and soft tissues), including the anatomical areas through which muscular and skeletal forces are transferred. The directions and magnitudes of these forces in the three-dimensional space, which are functions of the activity performed (e.g., gait, running, jumping, etc.), are also basic factors that determine the stress state of the foot.

The latest quantitative models that have analyzed the human foot as a mechanical structure used various simplifying assumptions concerning its geometry, mechanical properties of its tissues, and muscle loading. Nakamura [1] used a two-dimensional Finite Element (FE) model in an attempt to predict the stress states within the plantar soft tissue of the human foot for different shoe conditions. In his work, a single elastic body represented the complex bony structure of the foot with its articulated joints. A major breakthrough was achieved by Simkin [2], who developed a static model of the foot during standing, using matrix structural analysis. This model was both representative and quantitative in the three dimensions. However, as some joint geometric misrepresentation could not be avoided when using matrix structural analysis, the resulted reduced accuracy in the field of displacements did not allow a complete validation of the model. More complex models of similar concept, consisting of hinge joints, springs, and dampers to represent viscoelastic behavior, were recently suggested by Gilchrist et al. [3,4].

Chu et al. [5] presented an asymmetric three-dimensional FE foot model for analysis of ankle-foot orthosis effects. Linear elastic ligaments and soft tissue were included in this model, yet, the complex articulated structure of the foot skeleton was treated as a single body. The recent two-dimensional FE model by Patil [6], used to study regions of high stress in normal and neuropathic feet during gait, was constructed according to the two-dimensional cross-sectional anatomy of the foot, obtained from a lateral X-ray image; although their work is an important step toward the ability to predict structural stress concentrations in normal and disordered feet, the two-dimensional approach limits the model validity. In the latest three-dimensional FE model of Patil's group [7], bones of the medial and lateral arches in the medio-lateral directions are combined, forming, nonetheless, a simplified foot structure.

Some enhancement in the simulation of foot behavior was recently achieved by using a five planar sections approach [8,9], in which each of the five foot rays is modeled as an individual two-dimensional structure. Nevertheless, this methodology cannot account for the three-dimensional interlinks among the foot skeletal components. One may conclude from the above-mentioned recent studies that a state-of-the-art model of the human foot for analysis of structural stresses during gait is still missing and should be

Contributed by the Bioengineering Division for publication in the JOURNAL OF BIOMECHANICAL ENGINEERING. Manuscript received by the Bioengineering Division September 22, 1999; revised manuscript received July 9, 2000. Associate Technical Editor: M. L. Hull.

developed according to real, highly accurate three-dimensional *in vivo* skeletal geometry, including the three-dimensional anatomical cartilaginous articulations. Ligaments and soft tissues should also be considered and their nonlinear biomechanical behavior must be based on experimentally obtained data. Furthermore, the model should be validated by comparing its predictions with experimentally obtained kinematic/dynamic data, recorded during natural gait.

Therefore, in the present study, a complex three-dimensional FE model of a normal foot structure, including cartilage and ligaments for simulation of realistic joint articulations, is developed for the first time in the literature, in discrete events during the stance phase of gait. The development of this realistic three-dimensional foot model requires *in vivo* information on the relationship of foot skeletal motion during stance to the resultant Foot-Ground Pressure Pattern (FGP). In order to obtain such information, a novel experimental gait analysis technique had also to be developed and consequently used in this study. As further presented, this technique integrates two measurement methods: Contact Pressure Display (CPD) and Digital Radiographic Fluoroscopy (DRF). The CPD/DRF integrated experimental analysis is able simultaneously to yield both the kinematic and dynamic structural behaviors of the foot during gait, including the FGP, needed for the development and validation of the three-dimensional FE model.

The information provided by the foot model on the regions of high stresses in the foot further allows numerous medical applications, toward diagnosis and prognosis. For example, locating sites of highly elevated stresses in the foot during gait is of major clinical importance in understanding the development mechanisms of stress fractures [10], arthrosis [11], or diabetic ulcers [9,12,13]. Simulation of structural disorders and their surgical correction, e.g., presurgical evaluation of the biomechanical effects of an internal fixation used to treat skeletal fractures, are also possible applications of the newly developed foot model.

Experimental Methods

The Contact Pressure Display (CPD) Method. The CPD is an optical method developed by Arcan and Brull [14–17] for quantitative plantar pressure measurements (see also [2,9,10,13,18–21]). According to this method, a birefringent integrated optical sandwich was built and used for analysis of the foot-ground contact pressure distribution. The total transferred load is discretized into contact points by a matrix of independent pins with spherical tips. Using monochromatic polarized light, concentric isochromatics appear under every contact point and their maximal diameter is a calibrated function of the local contact load. The contact pressure images were acquired using a high-resolution 0.5 in. CCD camera (Chiper, CPT-8360). A digital video capture board (Miro 20TD), installed in a PC, was used to store the images for later processing using a specifically developed software, in order to obtain quantitative patterns of pressure distribution. The CPD method was selected to be used in the present research for plantar pressure evolution measurements because of its ability to yield a simultaneous, fast imaging process of the whole contact area; moreover, the optical multisensor device could be easily adapted for the further proposed integrative system.

The Digital Radiographic Fluoroscopy (DRF) Method. The DRF method is a computerized X-ray based examination that displays and electronically records skeletal and soft tissue motion, providing the positions of the foot bones and joints during gait. The Philips Multi Diagnost 3 (MD3) DRF system, located at the Diagnostic Imaging Dept., Sheba Medical Center (Tel Aviv), was used for the experiments. The MD3 is a maneuverable multifunctional, fully digital and highly accessible X-ray system, usually used for vascular/nonvascular (e.g., gastrointestinal) diagnostic interventional procedures and radiographic fluoroscopy examina-

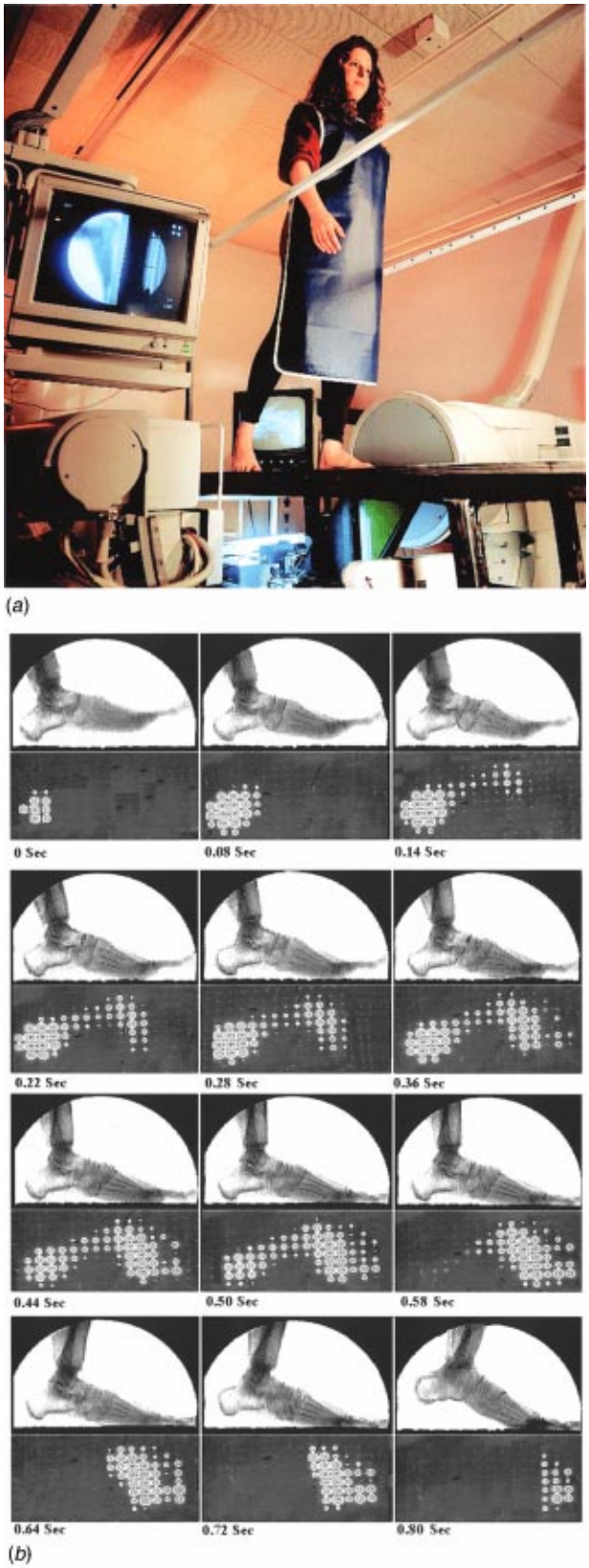

Fig. 1 The CPD/DRF integrated experimental analysis: (*a*) the experimental setup and (*b*) representative CPD/DRF data of a normal foot structure during various discrete stages of the stance phase; gait velocity 0.5 m/S. Time intervals are different between frames to present the most characteristic/descriptive subphases of the stance

tions. The MD3 offers an immediate image display during acquisition, as well as viewing, reviewing, and image storage options. It also includes a remote control panel, a dual-wedge filter in the X-ray tube's collimator for improved image quality and a DSI (Digital Spot Imager) (Philips) for automatic on-line optimization of images, during acquisition. The C-arm's rotation, angulation, and scanning movements allow projections from various positions and angles.

The CPD/DRF Gait Platform. Integrating the two measurement systems, foot-ground CPD and DRF, a basis condition of simultaneous data recording, was implemented, setting up a large field of applications. The contribution of each segment to the structural behavior of the foot may be studied by applying image processing and numerical analysis techniques. A CPD/DRF gait platform of 2.5 m length was mounted on the MD3 examination table (Fig. 1(*a*)). A computer-aided digitizing method of the foot's motion during the stance phase of gait was developed, to investigate the relationships of structural kinematic data to dynamic plantar pressure. The integrated CPD/DRF measurements provided the detailed skeletal motion and joint behavior of the foot simultaneously with the evolution of the plantar pressure pattern during the stance phase of gait, as shown in Fig. 1(*b*).

The Model

Building the Foot Three-Dimensional Skeletal Geometry. The foot bones were initially modeled as individual parts. The three-dimensional geometry of each bone was obtained using a surface generation software (SURFdriver, Moody & Lozanoff), which created a detailed morphological reconstruction of the anatomical structure. Open MRI coronal images of the feet of a 27-year old male and a 25-year old female, as well as cryosection coronal foot images of a 39-year old male (The Visible Human Project, U.S. National Library of Medicine, http://www.nlm.nih.gov/) were used to obtain the three-dimensional shape of each bone in the foot skeleton. The relative positions of the modeled bones were then determined from sagittal Open MRI image slices of these subjects to conform to published anatomical data [22]. Particular attention was given to the surface geometry of the ankle, talocalcaneal, calcaneocuboidal, and talonavicular articulations.

The present foot model, shown in Fig. 2, consists of a total of 17 bony elements, which are interconnected by cartilaginous joints. Proximal, middle, and distal phalanges were unified in each toe for simplification, due to computational limitations of the FE solver. This assumption is not expected to yield significant inaccuracies in the predicted stress distributions, since during normal gait, at a moderate velocity, the contact stresses applied to the forefoot do not flex the interphalangeal joints [23]. Based on anatomical data, the bones and cartilage forming each joint are constrained to move by respective longitudinal ligaments, modeled on both the dorsal and plantar aspects. Transverse ligaments, linking the medial and lateral arches, were also introduced. A total of 15 dorsal ligaments, 15 plantar ligaments, 4 transverse ligaments, 2 ligaments at the talocalcaneal joint, 2 components of the long plantar ligament, and 5 components of plantar aponeurosis are thus incorporated in the model. The soft tissues on the plantar surface of the foot also play a significant role in determining the dynamic structural behavior, by providing a cushion between the ground and the skeletal system. A pad of soft tissue was therefore included in the model, covering the plantar aspects of the calcaneus, fourth, and fifth (lateral) metatarsal bones and the five metatarsal heads.

Material Properties. A significant difficulty for anatomical models resides in selection of the biological material properties, which are most often dependent on the nature of the applied load, e.g., the loading rate [24]. In the present analysis, a quasi-static loading system is applied to the foot model, by adding inertial forces to the body load, as discussed in the following sections.

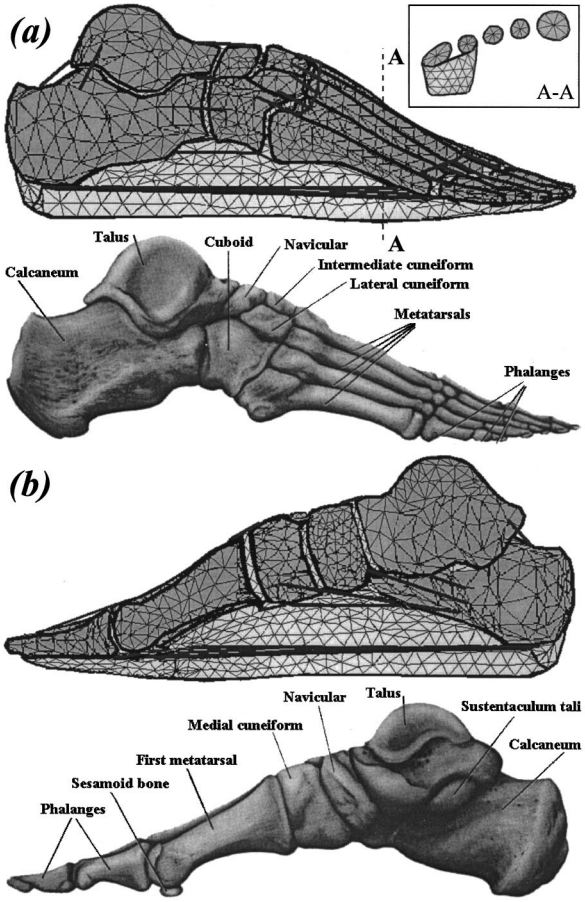

Fig. 2 The FE mesh of the three-dimensional model versus skeletal anatomy (adapted from [57]): (*a*) lateral view (A-A is a cross section through the center of the metatarsals) and (*b*) medial view

Huiskes [25] reported that in the case of quasi-static loading, both cortical and trabecular bones may be considered as having linearly elastic behavior. Moreover, under quasi-impact loading, useful information can be gained by correspondingly modeling joint cartilage as a linear elastic material [26]. Consequently, in the present model, bone and cartilage materials are assumed to be homogeneous, isotropic, and linear elastic. For the foot bones, Young's modulus is taken as 7300 N/mm^2 and the Poisson ratio as 0.3 [1]. For the cartilage, Young's modulus and Poisson ratio are taken as 1 N/mm^2 and 0.1, respectively [27,28]. The ligaments, plantar fascia, and soft tissue fat pad were considered nonlinear. The typical experimental load-deflection relationship used to model the ligaments was obtained by Race and Amis [29] through Instron uniaxial tensile tests on healthy, normal lower-limb ligaments. The following expression was fitted to the experimental data for the computational procedure:

$$P_l = a_l\delta^3 + b_l\delta^2 + c_l\delta + d_l \quad (1)$$

with a correlation coefficient of $R^2=0.995$, whereas P_l is the ligament load in kN, δ is the elongation in percent and the constants are $a_l=-4.09$, $b_l=5.388$, $c_l=0.287$, $d_l=0.0017$. The stiffness curve of the plantar fascia was taken as 70 percent of the ligament stiffness. This correction to the fascia's stiffness values, which was obtained in a convergent process of calculating the model stress state and correcting the load-displacement curve, satisfies the following condition: Under loading, no tensile forces are taken by the cartilage. The stresses that pass through the cartilage are all compressive or (nearly) zero, just as in reality [6,8].

The mechanical behavior of the soft tissue that pads the bony structure of the foot was taken from Nakamura [1], who obtained the uniaxial compression stress-strain curve of a specimen taken from the heel of a fresh cadaver. The following relationship was fitted to Nakamura's data:

$$\sigma_s = a \exp(b\varepsilon) \tag{2}$$

with a correlation coefficient of $R^2=0.99$, whereas σ_s is the fat pad stress in MPa, ε is the resulted strain and the constants are $a=0.006$ and $b=10.1$. This relationship was subsequently used in the present work for the soft tissue model; the Poisson ratio for the soft tissue (0.49) was also taken from the same work.

Numerical Method of Analysis. The FE method was selected for numerical analysis of the model due to its unique capability to analyze structures of complex shape, loading, and material behavior. The model was elaborated using the ANSYS 5.3 High-Option FE software package, developed by SAS, U.S., 1996. This powerful version enables generation of up to 32,000 nodes. Automatic division was used to generate an optimal mesh of 3645 solid structural elements that described the curved geometry of bones, cartilage, and soft tissue, as well as 240 rod elements building the ligaments. This mesh was determined by a converging process in which the mesh density was gradually increased, until the deviation in the produced stress values did not exceed 5 percent. During the meshing process, special attention was given to avoid extreme transitions in sizes of adjacent elements, which may induce local inaccuracies in the numerical solution. The selected eight-node elements allowed for large deflections and large strains. Each node has three degrees of freedom, i.e., translation in the *x*, *y*, and *z* directions, a state which is compatible with bending stresses. A nonlinear analysis of up to 25 equilibrium iterations was performed for each loading case, using the Newton-Raphson method.

Adaptation of the Model to the Subphases of Stance. Different terms are used in the literature to define the positions of the foot during the stance phase of gait. It is generally accepted to define three characteristic positions, i.e., heel strike, midstance, and push-off [30]. Some textbooks also define one or two additional intermediate positions [31] such as heel-rise (between midstance and push-off) and toe-off (following push-off). Since the present analysis requires a highly detailed description of the foot motion during stance, it was decided to define a series of six sequential characteristic subphases, which were termed as follows: (1) initial-contact, (2) heel-strike, (3) midstance, (4) forefoot-contact, (5) push-off, and (6) toe-off. This presentation of the stance phase integrates the common literature definitions with two new terms, Initial-Contact and Forefoot-Contact.

Initial-contact describes the position of the foot during its very early interaction with the ground, when only a small part of the heel plantar area is in contact (e.g., see the first frame in Fig. 1(*b*)); subsequently, heel-strike denotes the position of the foot when the heel is in full impacting contact with the ground (e.g., the second frame in Fig. 1(*b*)). It was decided to introduce an Initial-Contact subphase, before the Heel-Strike develops, in order to be able to record the whole evolution and time length of the stance, up to Toe-Off. Forefoot-Contact, an intermediate event between midstance and push-off, is the position in which both the forefoot and the anterior part of the midfoot (arch) are in contact with the ground. The model was adapted for each of the above-mentioned subphases by altering its skeletal/muscle loading characteristics and its geometric positioning (including both its gross inclination and the alignment of the phalanges in respect with the metatarsal bones). The six configurations of the foot model in the sagittal plane are given in Table 1 and Fig. 3, as related to their time of occurrence, which is expressed in percentage of the gait cycle; the timings are approximated, according to experimental analyses of the evolution of the foot–ground contact area during gait [21,30–33]. Adaptation of the structural and muscle loading system for each subphase is discussed in details in the next paragraphs.

Table 1 Kinematic characteristic data during the stance phase of normal gait. Parentheses indicate range of values (min-max).

	Initial-Contact	*Heel-Strike*	*Midstance*	*Forefoot-Contact*	*Push-Off*	*Toe-Off*
Timing [Sec] - function of velocities, between 0.5 to 0.9 [m/Sec]	0	(0.02 - 0.10)	(0.20 - 0.40)	(0.30 - 0.60)	(0.35 - 0.65)	(0.40 - 0.75)
Inclination of the Foot [Deg] in the Sagittal Plane *	(13 - 17)	(8 - 11)	0	(-7 - -4)	(-11 - -8)	(-21 - -15)

* + Dorsiflexion / - Plantar flexion

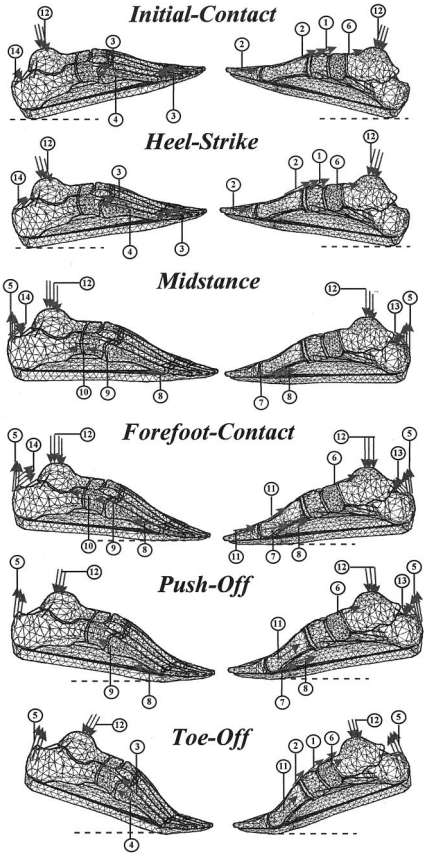

Fig. 3 Muscle forces that act on the foot model during the six characteristic subphases of stance (indicated by numbers 1–14 according to Table 1)

Loads and Constraints. An approximate method of treating dynamic loading during gait is a quasi-static approach, by adding inertia forces to the body weight. The above-described foot model was developed, in its six configurations, while taking into account these inertia forces according to literature reports.

Several muscles are responsible for foot movement during gait. Some of these muscles are characterized by very long tendons; they are located in the lower leg and produce dorsal and plantar flexion. As these muscles are attached to bones of the foot (via tendons), they obviously contribute to generating internal stresses within its structure. During locomotion, several muscles act predominantly on the foot. These muscles are the Tibialis Anterior (TA), Extensor Hallucis Longus (EHL), Extensor Digitorum Longus (EDL), Triceps Surae (TS), which include both the gastrocnemius and soleus, Tibialis Posterior (TP), Flexor Hallucis Longus (FHL), Flexor Digitorum Longus (FDL), Peroneus Longus (PL), Peroneous Brevis (PB) and the Abductor Hallucis (AH). The values of forces developed on each of the muscles during the

Table 2 The active muscle and structural loads acting on the model during the stance phase

#		*Initial-Contact* [N]	*Heel-Strike* [N]	*Midstance* [N]	*Forefoot-Contact* [N]	*Push-Off* [N]	*Toe-Off* [N]
1	Tibialis Anterior (TA)	267	535	-	-	-	267
2	Extensor Hallucis Longus (EHL)	212	424	-	-	-	212
3	Extensor Digitorum Longus (EDL)	186	372	-	-	-	186
4	Peroneus Tertius (PT)	9	17	-	-	-	9
5	Triceps Surae (TS)	-	-	550	825	1100	300
6	Tibialis Posterior (TP)	187	94	110	222	258	222
7	Flexor Hallucis Longus (FHL)	-	-	923	623	322	-
8	Flexor Digitorum Longus (FDL)	-	-	16	8	4	-
9	Peroneus Longus (PL)	-	-	1164	1185	1206	-
10	Peroneus Brevis (PB)	-	-	66	33	-	-
11	Abductor Hallucis (AH)	-	-	-	110	55	27
12	Ankle Joint Load (AJL)	675	1350	2100	2550	3000	300
13	Reaction at the medial pulley	-	-	645	755	865	-
14	Reaction at the lateral pulley	358	716	256	128	-	-

stance phase of gait were taken from the literature [6,7,34–38]. Since it is not feasible to measure muscle forces *in vivo*, muscle forces were predicted in most of these works using optimization techniques, according to some physiological parameters, such as muscle cross-sectional area, muscle mass, muscle fiber length, muscle length, etc. Since these parameters differ significantly among subjects and are highly dependent on body structural characteristics and gender, differences reaching up to 30 percent in magnitudes of muscle forces generated in the lower limbs were observed in the normal, healthy population [35]. In order to study the present foot model numerically, it was necessary to determine a set of strict muscle loads that are active at each stance position, in a quantitative way. Therefore, during the development process, the model was repeatedly solved at each stance position in a converging trial and error procedure. Different muscle forces within the normal range were applied to the structure until validation, in terms of optimal agreement between numerically predicted and experimentally measured plantar pressures was achieved (see the following section, Model Validation). In the absence of literature data on some muscle forces that are developed in the newly defined stance positions (initial-contact and forefoot-contact), extrapolation/interpolation values were calculated as first approximations, using the nearest known magnitudes [35] as reference values; these interpolation values were also corrected within the normal 30 percent range, similarly to the muscle force values available from the literature, to obtain the best accord between computed and measured plantar pressures. The muscle forces used for the stress analysis are detailed in Table 2.

The Ankle Joint Loads (AJL) at the different stance stages were adapted from the works of Seireg and Arvikar [39] and Röhrle [40] for a normal body weight of 600 N. Since ankle joint reactions are also significantly different (25 percent) among subjects and highly dependent on body characteristics, gender, and gait velocity [41], optimal AJL values were again selected in a converging trial & error process meant to achieve successful validation.

The medial part of the calcaneus (*sustentaculum tali*), with its groove underneath, acts as a medial pulley for the TP, FDL, and FHL; a less predominant but similar bony protuberance, with similar location at the lateral side of the calcaneus, serves the PL and PB [7]. The effect of this mechanism, called the lateral pulley, appears at the lateral surface of the calcaneus, although the insertion of PL is on the medially located first cuneiform; the PL muscle crosses the foot at its plantar aspect.

Instead of attaching the muscles to single points, their loads are spread over the areas of their anatomical insertion regions [22] to avoid nonrealistic stress concentrations at the muscle attachment surfaces and thus, mimic the real muscle tendon/bone interaction. A useful approach to achieve this aim is to equally divide each total muscle force applied at a certain subphase (Table II) to smaller loads of 10-25 percent of the total load, depending on the magnitude of the total force and the size of the insertion region [7]; these smaller loads are distributed as evenly as possible over the insertion surface. The ankle joint load is similarly distributed to loads equaling 10 percent of its total value, located along the sagittal and medio-lateral directions. The forces on the calcaneus due to the muscles FHL, FDL, and TP as they contract around the medial pulley are also considered in the model, as well as the forces applied by PL and PB around the lateral pulley. Figure 3 shows the directions and insertion surfaces of active muscle forces and other loads acting on the foot model (Table II) at each of the stance positions [42].

Model Validation. The reaction forces generated during the foot-ground interaction and their evolution during gait are some of the most important biomechanical gait parameters, characterizing foot function [16,32,43–45]. The time-dependent reactions are composed of one vertical component and two horizontal components, for the longitudinal and lateral directions. In order to validate the foot model presented, numerical predictions of the evolution of these three components, as well as of the pressure distribution beneath the foot during the stance phase can be obtained and compared with experimentally acquired data; the resulting distributions of vertical reaction forces on the plantar area of the foot model for the six selected characteristic positions are shown in Fig. 4(*a*). Nevertheless, in order to obtain a comprehensive validation of the model, which will be based not only on analysis of its predictions with respect to dynamics of specific feet, but will also allow comparison with statistical data of sub-

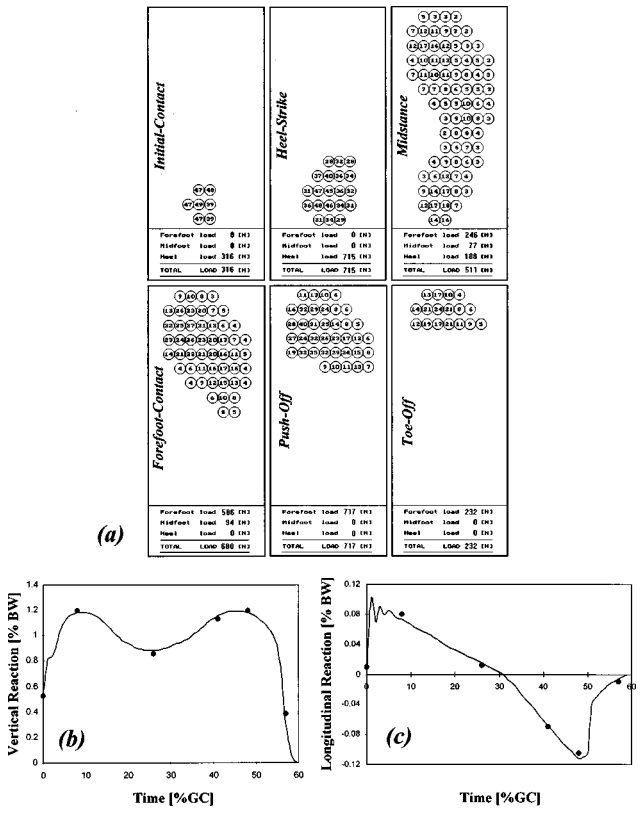

Fig. 4 Model validation: (*a*) the predicted distribution of vertical reaction forces [N] among the supports of the foot model at the six characteristic subphases of stance; (*b*) the predicted normalized total vertical reaction component, and (*c*) the predicted normalized total horizontal component in the longitudinal direction during stance versus typical measured data (adapted from Brull and Arcan [16]), obtained at a gait test of a normal subject (solid line)

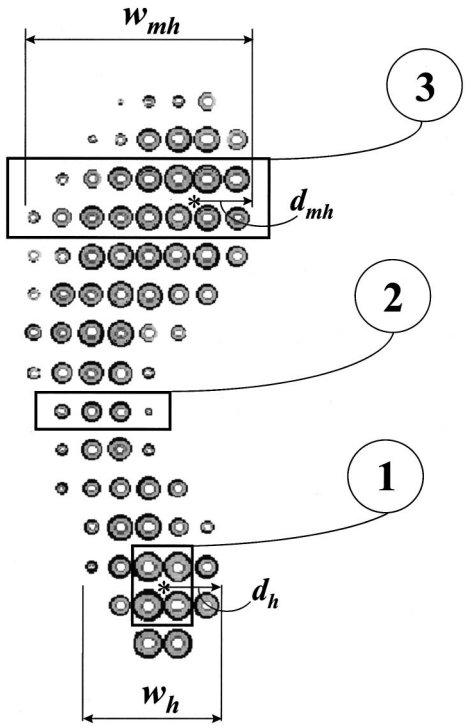

Fig. 5 Definition of the Stress Intensity Parameters (SIP) on a characteristic foot-ground CPD pattern: The highest loaded areas (1), (3) are selected to represent the heel sharpness and metatarsal head pressures respectively, while the lowest loaded area (2) is selected to represent the arch rise.

jects with different gender/body characteristics, a new technique for dimensionless characterization of the FGP evolution had to be developed.

A set of static contact pressure parameters, called Stress Intensity Parameters (SIP), were introduced by Brosh and Arcan [10] to provide not only a dimensionless description of the foot static structure as an arch, but also a quantitative mechanical characterization of its structural behavior. The Brosh and Arcan set of static SIP succeeded to characterize the foot structure during standing and to prove its sensitivity and tendency to stress fracture [10]. Statistical correlation was successfully established between critical values of the SIP and the prevalence of stress fractures among young subjects. The above-mentioned static set of SIP were adapted for the dynamic case as follows: for the heel,

$$h=\frac{\sigma^{h}_{\text{sharp}}}{\sigma_{\text{avg}}} \tag{3}$$

for the midfoot,

$$m=\frac{\sigma^{m}_{\text{min}}}{\sigma_{\text{avg}}} \tag{4}$$

and for the forefoot,

$$f=\frac{\sigma^{f}_{mh}}{\sigma_{\text{avg}}} \tag{5}$$

where σ_{avg} is the transient average foot-ground pressure, calculated as the midstance load transmitted by each foot, divided by the respective contact area; $\sigma^{h}_{\text{sharp}}$ is the transient average pressure on a square of four adjacent maximally loaded contact points, characterizing the heel of each foot (area 1 in Fig. 5); σ^{m}_{min} is the transient average pressure on a minimally loaded transverse strip under the arch, during the midstance subphase, characterizing the arch rise of each foot (area 2 in Fig. 5); σ^{f}_{mh} is the transient average pressure on two adjacent maximally loaded transverse strips, characterizing the metatarsal heads area of each foot during the push-off subphase (area 3 in Fig. 5).

Table 3 Dynamic Stress Intensity Parameters (SIP): experimental results versus model predictions

	Initial-Contact	*Heel-Strike*	*Midstance*	*Forefoot-Contact*	*Push-Off*	*Toe-Off*
			CPD Measurements			
h	7.02 (*sd*= 1.20)	7.50 (*sd*=1.22)	2.28 (*sd*=0.58)	-	-	-
m	-	-	0.78 (*sd*=0.30)	1.19 (*sd*=0.35)	-	-
f	-	-	1.23 (*sd*=0.26)	2.62 (*sd*=0.32)	3.42 (*sd*=0.31)	2.21 (*sd*=0.35)
e_h	-	0.02 (*sd*=0.02)	0.04 (*sd*=0.02)	-	-	-
e_{mh}	-	-	0.21 (*sd*=0.06)	0.18 (*sd*=0.06)	0.16 (*sd*=0.06)	-
			Model Predictions			
h	6. 81 (NS)	7.23 (NS)	2.14 (NS)	-	-	-
m	-	-	0.70 (NS)	1.25 (NS)	-	-
f	-	-	1.08 (P<0.01)	2.65 (NS)	3.32 (NS)	2.10 (NS)
e_h	-	0. 03 (P<0.01)	0.03 (P<0.01)	-	-	-
e_{mh}	-	-	0.19 (NS)	0.19 (NS)	0.18 (NS)	-

* Significance was set at the 5% level.
** *sd*, Standard Deviation; NS, Non Significant.

In view of the findings of Brosh and Arcan [10], this dynamic characterization of the foot structure using SIP may enhance screening and classification of subjects with tendency to develop stress fractures (for sports, military training, and other activities involving marching exercises) according to characteristic parameters of the foot-ground pressure diagrams. In addition to the previously defined SIP, two new parameters were introduced, defining the medio-lateral eccentricities of the Center of Pressure (COP) for two specific regions of interest, under the heel (e_h) and the metatarsal heads (e_{mh}):

$$e_h=\frac{1}{2}-\frac{d_h}{w_h} \tag{6}$$

$$e_{mh}=\frac{1}{2}-\frac{d_{mh}}{w_{mh}} \tag{7}$$

where, as marked on Fig. 5, w_h and w_{mh} are the transverse widths of the contact areas under the heel and metatarsal heads, respectively, while d_h and d_{mh} are the transverse distances of the COP from the medial boundaries of the contact areas under the heel and metatarsal heads respectively (Fig. 5). Hence, positive values for e_h and e_{mh} indicate medial eccentricities while negative values indicate lateral eccentricities.

The SIP of three male (76, 90, 73 kg) and three female (57, 60, 54 kg) normal, young healthy subjects were calculated from a statistical set of totally 36 dynamic CPD measurements (Table 3), taken at gait velocities ranging from 0.5 to 0.9 m/s. The specially built CPD/DRF gait platform at Sheba Medical Center was used to record 8 stance phases. However, since the length of the gait platform at Sheba had to be limited to 2.5 m and its optical sensor area to 0.60 m $\times$ 0.40 m, due to the physical structure of the DRF examination system, additional 28 measurement sets were taken at the Biomechanics Laboratory, Faculty of Engineering, Tel Aviv University (TAU), using a unique 7.5 m CPD gait platform. This platform provides a large optical sensor area (2.00 m long $\times$ 0.60 m wide) for a double step follow up, not only permitting the subjects to walk at greater velocities but also allowing more natural gait patterns by eliminating the need to train subjects to step on specific sensitive regions. Complementary systems that are integrated with the CPD gait platform at TAU, including a built-in piezoelectric force plate (Kistler, 0.60 m long $\times$ 0.40 m wide) and a body kinematics measurement system (Selspot) aimed to analyze both the movements and the inertia forces. The TAU platform provided further means for higher gait velocities and analysis.

The SIP values obtained from the above-mentioned 36 CPD data sets were compared with the foot model solutions by statistical means, in order to achieve optimal agreement between numerically predicted and experimentally measured ground-reaction forces. A Student's *t* test was used for the statistical analysis, and significance was set at the 5 percent level. The results of the comparison for different stance positions are given in Table 3.

The agreement between the measured SIP values and the model predictions appears to be very good. No statistically significant differences exist between the experimental data and the numerically predicted values in 11 out of the total 14 criteria selected for comparison (79 percent). The minor discrepancies, which are related to the eccentricity of the heel load during heel-strike and midstance, are mainly due to the fact that the present foot model was developed to represent a typical ''averaged'' foot structure, while the experimental SIP results were obtained from specific subjects. To illustrate this point, an additional *t* test, aimed at identifying statistical differences between SIP values obtained from male and female subjects, was performed. This gender-dependency test showed that the average heel sharpness parameter during heel-strike was significantly higher ($p<0.01$) for the male group ($h=8.1\pm1.2$) compared with the female group ($h=6.8\pm0.5$), indicating greater impact forces, mainly due to the body weights, contributing to higher impact on the heel-pad during heel-strike in males. Thus, through statistical comparison of the dynamic SIP, measured from a group of six subjects, with the SIP predicted by the model at different positions during stance, the validation process could be further executed.

Both CPD measurements and the model show that COP eccentricities at the contact regions under the heel and metatarsal heads maintain positive values, i.e., medial orientation, during the whole stance phase (Table 3). Under the heel, COP values are only slightly displaced toward the medial aspect in an approximately constant shift of 0–6 percent. Under the metatarsal heads, pressures are medially orientated in a more pronounced shift (15–27 percent). These COP eccentricities under the heel and metatarsal heads were shown to be consistent in normal, healthy subjects. Abnormal foot structures or gait patterns, which are likely to alter the later characteristic COP trajectories [44], may be consequently characterized using the present SIP approach.

The dynamic SIP calculated in the present study for the midstance stage of male subjects were compared with the static results obtained by Brosh and Arcan [10] for 22 healthy, young male subjects during standing. The presently obtained dynamic midfoot minimum (*m*) was found to be greater by approximately 30 percent, when compared with the static results in the literature. This result may be well expected when considering the tendency to flattening of the arch during midstance [21], which is obviously reflected by the present dynamic SIP values.

The predictions provided by the model for the horizontal components of the foot-ground reaction force can be validated through comparison to experimental results obtained using a Kistler piezoelectric force platform [16]. The sagittal component is of special clinical interest, since it generates shear stresses both in the plantar soft tissues and in the shoe sole during the stance phase of gait, thus playing an important role in the development process of some foot disorders, e.g., diabetic ulcers [12]. The normalized (percent BW) evolutions of the predicted vertical and sagittal reaction components through the six subphases of stance (Fig. 4(*b, c*)) are shown to conform (maximum difference 8 percent) to typical experimental data measured by Brull and Arcan [16] during gait tests of a healthy subject, hence further validating the model.

Results

Basics. In order to achieve the three-dimensional foot structural analysis, the following set of biomechanical tools was developed:

1 A system of experimental methods for data acquisition during gait, integrating an optical method for plantar pressure measurements (CPD) and a digital fluoroscopic instrument (DRF) for skeletal motion simultaneous recording.

2 A Stress Intensity Parameter (SIP) system for dynamic evaluation and characterization of the foot and gait individual behavior. A statistical approach based on the Dynamic SIP development also allows to characterize specific gait of various groups (e.g., differing by age, gender, etc.) or human activities involving marching exercises like military training and some sports.

3 A three-dimensional numerical model of the foot has been developed, incorporating realistic geometric and material properties of both skeletal and soft tissue components of the foot, for biomechanical analysis of its structural behavior during gait.

The first two results are very important, not just for a most complete gait-data-base acquisition and evaluation, but mainly for the model building and its mechanical validation. Obviously, many significant clinical applications are now possible. For instance, the foot model may provide the surgeon some simulated pre-operative alternative foot corrections, including their model-simulated biomechanical effects and thus, assist him toward his final decision.

Model Simulation Results. The model was applied to obtain the stress distribution within the foot structure during the defined six subphases of stance (Fig. 6). Results of the FE analysis are presented in terms of von Mises equivalent stresses ($\sigma_{\text{v.M.}}$), which weight the effect of all principal stresses (σ_1, σ_2, σ_3) according to the relation:

$$\sigma_{\text{v.M.}}=\left\{\frac{1}{2}[(\sigma_1-\sigma_2)^2+(\sigma_2-\sigma_3)^2+(\sigma_3-\sigma_1)^2]\right\}^{\frac{1}{2}} \tag{8}$$

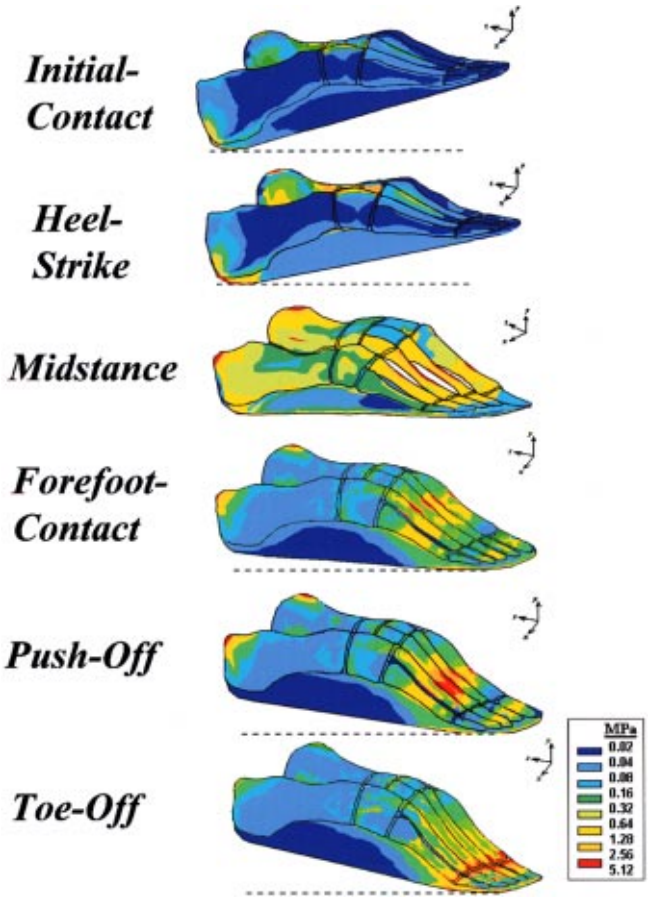

Fig. 6 The von Mises stress distributions in the foot model at the six characteristic subphases of stance

Table 4 Sites of elevated von Mises stresses located on the foot model during the stance phase

Stage	Sites of Elevated Stresses			Respective Max Stress Values [MPa]		
Initial-Contact	calcaneus (*Pl*);	calcaneus (*Ps-M*);	talus (*D*);	0.45;	1.21;	1.07;
	cuboid (*D*);	cuneiforms (*D*);	3rd metatarsal (*D*)	1.02;	0.88;	0.30
Heel-Strike	calcaneus (*M*);	talus (*D*);	cuboid (*D*);	1.24;	2.55;	1.79;
	cuneiforms (*D*);	3rd metatarsal (*D*)		1.56;	1.59	
Midstance	calcaneus (*Ps*);	talus (*D*);	talus (*L*);	3.48;	2.72;	2.61;
	1st-3rd metatarsals (*M-D*)			3.65		
Forefoot-Contact	calcaneus (*Ps*);	talus (*D*);	2nd, 3rd metatarsals (*D*)	3.18;	3.37;	4.17
Push-Off	calcaneus (*Ps*);	talus (*D*);	2nd, 3rd metatarsals (*D*)	3.80;	3.55;	4.46
Toe-Off	calcaneus (*Ps*);	talus (*D*);	1st-3rd metatarsals (*A-D*)	0.61;	1.04;	4.23

Pl - plantar , *D* - dorsal, *L* - lateral, *M* - medial, *A* - anterior and *Ps* - posterior aspects

Locations of elevated von Mises stresses, identified on the foot model for each of the above mentioned stance positions, are detailed in Table 4.

• The simulated stress distribution for the initial-contact and mainly for the heel-strike subphase show elevated stress sites, at the posterior-medial aspect of the calcaneus, due to the heel-ground impact. Raised stress values within the foot structure during heel-strike are also found on the dorsal aspect of the talus, which carries the dynamic body loads that are transferred via the tibio-talar joint; the central part of the arch, including the dorsal surfaces of the cuboid and the cuneiforms are also subjected to intensified stresses, due to contraction of the tibialis anterior, extensor hallucis longus, and extensor digitorum longus muscles, which act, together with the mechanisms of ligament stretch and joint motion, to absorb some of the heel-ground impact energy [46].

• Examination of the stress distribution, obtained for the midstance position, shows relatively high stresses at the talus, calcaneus, and medial metatarsals. The subtalar (talus-calcaneus) joint appears to be the most loaded joint during midstance. The ankle joint load, the triceps surae muscle force transferred via the Achilles tendon, as well as the reactions at the lateral and medial pulleys all exert a moment on the calcaneus. This moment is balanced in the subtalar joint, which divides the dynamic body load between the hindfoot and the forefoot. The maximal stress values and largest stress concentrations were found at the medial-dorsal aspects of the central part of the first three metatarsals, the dorsal and lateral aspects of the talus, and the posterior aspect of the calcaneus. During midstance, the principal stresses at the dorsal aspect of the foot skeleton are predominantly compressive in nature, mainly due to the flattening of the structure. In the plantar aspect, however, principal stresses are mostly tensile, since as the foot flattens, the plantar ligaments and fascia are stretched, locally transferring tension stresses to the anterior aspect of the calcaneus and to the plantar aspects of the metatarsal heads; these stresses transform themselves into the above mentioned dorsal compression, due to the arch effect. The long plantar ligament, for instance, exerts significant tension stresses (maximum 1.12 MPa) in the region of its insertion point on the anterior aspect of the calcaneus (Fig. 6) in its role to attenuate the dynamic shock wave, reduced by the combined function of plantar ligaments and fascia with approximately 10 percent [47]. This interaction, between soft and hard tissue components of the foot, should therefore be taken into account when considering the effect of trauma damage or surgical interventions involving release or removal of plantar ligaments or fascia.

• Simulation of the structural behavior of the foot during forefoot-contact, push-off, and toe-off subphases revealed elevated stress sites concentrated on the dorsal aspects of the first four metatarsals and phalanges, which carry most of the forefoot load at these positions, as demonstrated by the CPD/DRF tests (e.g., see Fig 1(*b*)). These sites are progressively shifted distally toward the end of stance, whereas the highest loaded region appears at the central part of the third metatarsal during push-off.

• The present analysis further shows that from forefoot-contact to toe-off, in most parts of the metatarsals, principal stresses are compressive, although in the most highly stressed regions there is also some tension present due to bending. While the metatarsals, generating the anterior aspect of the arch, carry increased loads from forefoot-contact to end of stance, the central part of the arch, i.e., the cuboid and lateral cuneiforms, bear significantly lower stress values (by a factor of approximately 2), compared to the stresses carried at the midstance stage. Additional sites of high stresses are found at the dorsal aspect of the talus that is continuously loaded with the dynamic body weight, as well as at the posterior aspect of the calcaneus, which is subjected to the contraction force of the triceps surae.

Discussion

General Comments. Several specific aspects of the above-described evolution of the stress distribution within the foot are supported by recent studies in the literature. The development of medially oriented calcaneal stresses during heel-strike may be well correlated with the findings of Rodgers [43,44], who demonstrated this phenomenon experimentally by statistically comparing lateral and medial heel-ground contact stresses. In the studies of Rodgers, mean pressures under the medial region of the heel were found to be approximately 20 percent greater than those under the lateral region. During midstance, the first three metatarsals are shown to transfer most of the forefoot load. This observation is well supported by our prior knowledge on the dynamic FGP patterns during midstance, obtained through the CPD/DRF measurements (e.g., see Fig. 1(*b*)), as well as by other studies in which contact pressure distributions were recorded using capacitive, resistive, or piezoceramic sensor arrays [44,48,49]. Our analysis further demonstrated that the highest loaded region during push-off appears at the center of the third metatarsal bone. This result is well supported by the findings of Scott and Winter [3], Rodgers [43,44], Hughes [50], and Hermann [51], who demonstrated, using pressure transducers, that maximal contact stresses under the central metatarsal heads (second, third, and fourth) during push-off are highly prevalent among normal individuals. A large-scale statistical research, conducted by Henning and Milani [52] with 111 normal subjects, showed that peak pressures beneath the third metatarsal head during push-off were higher than under the first and fifth metatarsal heads.

The numerical simulation predicted the highest stress values to appear in the dorsal part of the mid-metatarsals from midstance (maximum 3.48 MPa) to toe-off (maximum 4.23 MPa). Other high stress regions were found during these subphases at the posterior aspect of the calcaneus (maximum 3.84 MPa). Jacob [7] obtained higher stress values of up to 5.13 MPa for stresses at the central parts of the fourth and fifth metatarsals and 8.97 MPa for the anterior-dorsal aspect of the calcaneus during midstance, using a simplified model in which both the lateral metatarsals and the medial metatarsals were treated as single bodies and most of the midfoot joints were affixed. It is most likely that these later assumptions in Jacob's work would result in greater stress values, as the exclusion of several principal joints in his model produced an unnaturally stiff foot structure. Therefore, although some qualitative characteristics of Jacob's results (such as the ones indicating that the medial metatarsals and dorsal face of the talus are highly loaded during midstance) are in agreement with the present analysis, several differences, which are mainly related to the loading of the joints, exist between the results obtained from the two models. For instance, while Jacob's model indicated the junction of the calcaneus and cuboid to be the most loaded joint during midstance, the present analysis shows that the subtalar joint is the most loaded one.

It is most likely that such discrepancies appearing between the present results and the previous simplified two- or three-

dimensional models arise due to the last year's progress in the field of numerical modeling, which allowed the introduction of natural three-dimensional geometry of the foot structure, a more realistic location of muscle insertions, and many other modeling abilities. Hence, the present three-dimensional numerical model was shown not only to react according to experimental evidences, but also to provide, for the first time in the literature, an integral approach to the study of structural behavior of the foot during gait.

The structure of the human foot is extremely complex and accordingly, development of reliable experimental methods and realistic computational simulations describing its mechanical behavior during gait, is highly complicated.

In order to overcome the technical difficulties related with the computational limitations of the currently available commercial FE software packages, some simplifying assumptions were still required and should be kept in mind while interpreting the results. In the FE model, the mechanical properties of bone and cartilage tissues of the foot were assumed to remain constant in time and to be homogenous, isotropic, and linear elastic. This assumption is generally adequate for analysis of bones subjected to dynamic loading [1] but in the cartilage tissue, according to Fung [53], a quasi-linear viscoelastic assumption should be considered (see also [6,7,26]). It is possible that introduction of a more realistic approach, not only for the cartilage but also for the plantar tissue pad, will decrease the foot-ground reaction forces (due to energy attenuation) and thereby, impose use of larger muscle forces to obtain successful validation with experimental data. Finally, imaging of the foot motion during gait was performed only in the sagittal (and not in the transverse) plane, since the X-ray source and detector elements of the DRF system could not be positioned to enable measurement in this plane without disturbing locomotion. Therefore, the model still lacks input of the relative motion between bones in the transverse plane during the subphases of stance.

The ability to acquire data characterizing internal stress states and their evolution during gait makes the presented three-dimensional numerical model a basic clinical tool. Since the model can identify vulnerable skeletal and soft tissue components of the foot, it can be used not only for understanding the development mechanisms of some common disorders (like the ones associated with diabetes, arthritis, stress fractures, etc.), but also to serve as a tool for development of novel clinical decision making and foot treatment approaches, as discussed in the next sections.

Applications to Foot Surgery. As already mentioned, orthopedic surgeons frequently need objective information about the likelihood of success of a planned surgical intervention. The present foot model is able to provide such pre-operative evaluation by simulating the biomechanical effects of the intended surgical treatment. For example, in order to enhance structural foot corrections in diabetic patients [54], virtual removals of some bony and soft tissue elements from the model can be carried out until an optimal structure is obtained, in terms of functional behavior and stress distribution during gait. Routine management of this computational procedure prior to Transmetatarsal Amputations (TMA) in diabetes, for instance, may minimize skin breakdown, which is a common post-TMA complication among these patients [55], by reducing local soft tissue stresses.

Applications to Gait Physical Therapy. Clinical gait laboratories, employing physical therapy methods, are gradually becoming widely present in hospital settings. From a clinical-practical perspective, great benefits could be obtained by integrating both measurements and numerical analysis tools as presented in this paper. Clinical use of gait data generally takes the form of evaluating biomechanical and neuromuscular consequences following a specific treatment, which may be surgical, orthotic, prosthetic, or physical therapy. However, the current medical procedures used to obtain the data needed for these assessments (including physical examination, observations, radiographs, and plantar pressure diagrams) may provide only limited information regarding the efficiency of a specific treatment. Introducing the three-dimensional numerical model of the foot, which can be adapted for use with any method of contact pressure measurements, the present study provides new tools for foot diagnosis and prognosis, enabling quantitative evaluation of possible foot treatments. Physical therapists may consequently apply these tools to assess quantitatively the characteristic behavior of the foot components during gait while corroborating the findings using dynamic electromyography (EMG) signals of the lower extremity muscles. For example, lack of foot stability for certain patients could be perceived during one or more of the main subphases of stance, i.e., heel-strike, midstance, or push-off. This phenomenon may be correlated with abnormal lateral or medial deviations at the center of the respective FGP due to abnormal force output of one of the triceps surae muscles and the physical therapist can be guided by this information to the muscle that should be treated in the rehabilitation program. The measured kinematic/dynamic and EMG data can also be incorporated as input parameters for the three-dimensional foot model, to simulate both foot abnormality and the suggested treatment. Following treatment, CPD/DRF tests could be repeated, to compare predicted with actual results.

A common clinical use of gait analysis in physical therapy is to compare the performances of disabled individuals with normative data to describe how disabled gait differs from the ''normal.'' However, at the present stage, gait analysis methodologies are lacking standard normalization procedures that will optimize subject evaluation toward establishment of normative databases for disabled groups [56]. In this field, the previously suggested dynamic SIP approach seems to be applicable; the approach can be used in clinical research and practice not only to produce standard databases, but also to correlate the foot structure behavior quantitatively with its (dys)function.

Conclusions

These findings demonstrate that stress distribution within the foot structure during gait can be obtained using a realistic three-dimensional model, by combining two powerful techniques: integrative CPD/DRF measurements and Finite Element modeling. In each of the six subphases, the model was adapted according to data provided by the DRF kinematic measurements, in order to simulate the structural stresses within the foot skeleton and soft tissues. CPD measurements were used to validate the model by applying the newly introduced dynamic SIP characteristics. The resulting ground reaction forces and contact stresses, obtained for each of the six subphases, compared well with respective experimental data, when subjected to predefined statistical tests. Finally, the presently developed biomechanical tools open new approaches for clinical applications, from simulation of the development mechanisms of common foot disorders to pre- and post-interventional evaluation of their treatment.

Nomenclature

AJL = ankle joint load
COP = center of pressure
CPD = contact pressure display
DRF = digital radiographic fluoroscopy
DSI = digital spot imager
EDL = extensor digitorum longus
EHL = extensor hallucis longus
EMG = electromyography
FDL = flexor digitorum longus
FE = finite element
FGP = foot-ground pressure pattern
FHL = flexor hallucis longus
MD3 = multi diagnost 3 (Philips)
PB = peroneus brevis
PL = peroneus longus

SIP = stress intensity parameters
TA = tibialis anterior
TAU = Tel Aviv University
TMA = transmetatarsal amputations
TP = tibialis posterior
TS = triceps surae

References

[1] Nakamura, S., Crowninshield, R. D., and Cooper, R. R., 1981, ''An Analysis of Soft Tissue Loading in the Foot: A Preliminary Report,'' Bull. Prosthet. Res., **18**, pp. 27–34.
[2] Simkin, A., 1982, ''Structural Analysis of the Human Foot in Standing Posture,'' Ph.D. thesis, Tel Aviv University, Tel Aviv.
[3] Scott, S. H., and Winter, D. A., 1993, ''Biomechanical Model of the Human Foot: Kinematics and Kinetics During the Stance Phase of Walking,'' J. Biomech., **26**, pp. 1091–1104.
[4] Gilchrist, L. A., and Winter, D. A., 1996, ''A Two-Part Viscoelastic Foot Model for Use in Gait Simulations,'' J. Biomech., **29**, pp. 795–798.
[5] Chu, T. M., Reddy, N. P., and Padovan, J., 1995, ''Three-Dimensional Finite Element Stress Analysis of the Polypropylene Ankle-Foot Orthosis, Static Analysis,'' Med. Eng. Phys., **17**, pp. 372–379.
[6] Patil, K. M., Braak, L. H., and Huson, A., 1996, ''Analysis of Stresses in Two-Dimensional Models of Normal and Neuropathic Feet,'' Med. Biol. Eng. Comput., **34**, pp. 280–284.
[7] Jacob, S., Patil, K. M., Braak, L. H. and Huson, A., 1996, ''Stresses in a 3-D Two Arch Model of a Normal Human Foot,'' Mech. Res. Commun., **23**, pp. 387–393.
[8] Gefen, A., Megido-Ravid, M., Itzchak, Y., and Arcan, M., 1998, ''Biomechanical Evaluation of Surgical Plantar Fascia Release Effects,'' *Proc. VIII Mediterranean Conf. on Med. & Biol. Eng. & Comput.*, Limassol.
[9] Gefen, A., Megido-Ravid, M., Azariah, M., Itzchak, Y., and Arcan, M., 1998, ''Biomechanical Modeling of the Diabetic Foot Using Open MRI,'' *Proc. 11th Conf. of the European Society of Biomechanics*, Toulouse (also in J. Biomech., **31**, Suppl. 1, pp. 10).
[10] Brosh, T., and Arcan, M., 1994, ''Toward Early Detection of the Tendency to Stress Fractures,'' Clin. Biomech., **9**, pp. 111–116.
[11] Kitaoka, H. B., and Patzer, G. L., 1998, ''Arthrodesis for the Treatment of Arthrosis of the Ankle and Osteonecrosis of the Talus,'' J. Bone Joint Surg. Am., **80**, pp. 370–379.
[12] Cavanagh, P. R., and Ulbrecht, J. S., 1992, ''Biomechanics of the Foot in Diabetes Mellitus,'' *The Diabetic Foot*, M. E. Levin, L. W. O'Neal, and J. H. Bowker, eds., Mosby-Year Book, St. Louis, pp. 199–232.
[13] Gefen, A., Megido-Ravid, M., Azariah, M., Itzchak, Y., and Arcan, M., 1998, ''Integrating a Photoelastic Device into Open MRI for Soft Tissue Mechanics Studies,'' *Proc. 11th Int. Conf. on Experimental Mechanics*, Oxford.
[14] Arcan, M., and Brull, M. A., 1976, ''A Fundamental Characteristic of the Human Body and Foot, the Foot-Ground Pressure Pattern,'' J. Biomech., **9**, pp. 453–457.
[15] Arcan, M., and Brull, M. A., 1980, ''An Experimental Approach to the Contact Problem Between Flexible and Rigid Bodies,'' Mech. Res. Commun., **7**, pp. 151–157.
[16] Brull, M. A., and Arcan, M., 1984, ''Analytical and Experimental Models and Techniques in Posture and Gait Studies,'' *Modeling and Analysis in Biomedicine*, C. Nicolini, ed., Word Scientific Publishing Company, Singapore, pp. 509–539.
[17] Arcan, M.,1990, ''Non Invasive and Sensor Techniques in Contact Mechanics: A Revolution in Progress,'' Invited Paper, *Proc. 9th Int. Conf. on Experimental Mechanics*, Copenhagen.
[18] Cavanagh, P. R., and Mickiyoshi, A., 1980, ''A Technique for the Display of Pressure Distribution Beneath the Foot,'' J. Biomech., **13**, pp. 69–75.
[19] Arcan, M., Brull, M. A., Scholten, R., and Röhrle, H., 1981, ''A New Method for Determining the Active Force System in Lower Limbs During Human Locomotion,'' Z. Orthop., Ihre Grenzgeb, **119**, pp. 595–597.
[20] Debrunner, H. U., 1985, *Biomechanik des Fusses* (*Foot Biomechanics*), Enke, Stuttgart.
[21] Gefen, A., Megido-Ravid, M., Itzchak, Y., and Arcan, M., 1998, ''Integrating Computer Aided Radiography and Plantar Pressure Measurements for Complex Gait Analysis,'' *Proc. 27th Israel Conf. on Mechanical Engineering*, Haifa.
[22] Gray, H., 1995, *Gray's Anatomy*, Churchill Livingstone, Edinburgh.
[23] Saltzman, C. L., and Nawoczenski, D. A., 1995, ''Complexities of Foot Architecture as a Base of Support,'' J. Orthop. Sports Phys. Therapy, **21**, pp. 354–360.
[24] Gefen, A., Elad, D., and Shiner, R. J., 1999, ''Analysis of Stress Distribution in the Alveolar Septa of Normal and Simulated Emphysematic Lungs,'' J. Biomech., **32**, pp. 891–897.
[25] Huiskes, R., 1982, ''On the Modeling of Long Bones in Structural Analyses,'' J. Biomech., **15**, pp. 65–69.
[26] Clift, S. E., 1992, ''Finite-Element Analysis in Cartilage Biomechanics,'' J. Biomed. Eng., **14**, pp. 217–221.
[27] Liu, G. T., Lavery, L. A., Schenck, R. C., Lanctot, D. R., Zhu, C. F., and Athansiou, K. A., 1997, ''Human Articular Cartilage Biomechanics of the Second Metatarsal Intermediate Cuneiform Joint,'' J. Foot Ankle Surg., **36**, pp. 367–374.
[28] Athanasiou, K. A., Liu, G. T., Lavery, L. A., Lanctot, D. R., and Schenck, R. C., 1998, ''Biomechanical Topography of Human Articular Cartilage in the First Metatarsophalangeal Joint,'' Clin. Orthop., **348**, pp. 269–281.
[29] Race, A., and Amis, A., 1994, ''The Mechanical Properties of the Two Bundles of the Human Posterior Cruciate Ligament,'' J. Biomech., **27**, pp. 13–24.
[30] Cailliet, R., 1983, *Foot and Ankle Pain*, F. A. Davis Company, Philadelphia.
[31] Sammarco, G. J., 1989, ''Biomechanics of the Foot,'' *Basic Biomechanics of the Musculoskeletal System*, M. Nordin and V. H. Frankel, eds., Lea & Febiger, Philadelphia, pp. 163–181.
[32] Chan, C. W., and Rudins, A., 1994, ''Foot Biomechanics During Walking and Running,'' Mayo Clin. Proc., **69**, pp. 448–461.
[33] Rose, J., and Gamble, J. G., 1994, *Human Walking*, Williams & Wilkins, Baltimore.
[34] Wickiewicz, T. L., Roy, R. R., Powell, P. L., and Edgerton, V. R., 1983, ''Muscle Architecture of the Human Lower Limb,'' Clin. Orthop., **179**, pp. 275–283.
[35] Brand, R. A., Pedersen, D. R., and Friederich, J., 1986, ''The Sensitivity of Muscle Force Predictions to Changes in Physiologic Cross-Sectional Area,'' J. Biomech., **19**, pp. 589–596.
[36] Fukunaga, T., Kawakami, Y., Kuno, S., Funato, K., and Fukashiro, S., 1997, ''Muscle Architecture and Function in Humans,'' J. Biomech., **30**, pp. 457–463.
[37] Glitsch, U., and Baumann, W., 1997, ''The Three-Dimensional Determination of Internal Loads in the Lower Extremity,'' J. Biomech., **30**, pp. 1123–1131.
[38] Kawakami, Y., Ichinose, Y., and Fukunaga, T., 1998, ''Architectural and Functional Features of Human Triceps Surae Muscles During Contraction,'' J. Appl. Physiol., **85**, pp. 398–404.
[39] Seireg, A., and Arvikar, R. J., 1975, ''The Prediction of Muscular Load Sharing and Joint Forces in the Lower Extremities During Walking,'' J. Biomech., **8**, pp. 89–102.
[40] Röhrle, H., Scholten, R., Sigolloto, C., and Sollbach, W., 1984, ''Joint Forces in the Human Pelvis-Leg Skeleton During Walking,'' J. Biomech., **17**, pp. 409–424.
[41] Simpson, L. J., and Bates, B. T., 1989, ''The Effect of Running Speed on Lower Extremity Joint Moment During the Support Phase,'' J. Biomech., **22**, p. 1083.
[42] Carlsöö, S.,1972, *How Man Moves: Kinesiological Studies & Methods*, William Heinemann, London.
[43] Rodgers, M. M., 1993, ''Biomechanics of the Foot During Locomotion,'' *Current Issues in Biomechanics*, M. D. Grabiner, ed., Human Kinetics Publishers, Champaign, pp. 33–49.
[44] Rodgers, M. M., 1995, ''Dynamic Foot Biomechanics,'' J. Orthop. Sports Phys. Therapy, **21**, pp. 306–315.
[45] Soutas-Little, R. W., 1998, ''Motion Analysis and Biomechanics,'' in: *Gait Analysis in the Science of Rehabilitation*, T. T. Sowell, ed., Baltimore Rehabilitation Information and Technology Administrative Center, Baltimore, pp. 49–68.
[46] Salathe, Jr., E. P., Arangio, G. A., and Salathe, E. P., 1990, ''The Foot as a Shock Absorber,'' J. Biomech., **23**, pp. 655–659.
[47] Kim, W., and Voloshin, A. S., 1995, ''Role of the Plantar Fascia in the Load Bearing Capacity of the Human Foot,'' J. Biomech., **28**, pp. 1025–1033.
[48] Hughes, J., Clark, P., Linge, K., and Klenerman, L., 1993, ''A Comparison of Two Studies of the Pressure Distribution Under the Feet of Normal Subjects Using Different Equipment,'' Foot Ankle, **14**, pp. 514–519.
[49] Prutchi, D., and Arcan, M., 1993, ''Dynamic Contact Stress Analysis Using a Compliant Sensor Array,'' Measurement, **11**, pp. 197–210.
[50] Hughes, J., Clark, P., Jagoe, R., Gerber, C., and Klenerman, L., 1991, ''The Pattern of Pressure Distribution Under the Weightbearing Forefoot,'' The Foot, **1**, pp. 117–124.
[51] Hermann, B., 1995, ''Form and Structure of the Metatarsal Head Arch in Adults. Ultrasonographic and Podometric Studies,'' Z. Orthop. Ihre. Grenzgeb., **133**, pp. 335–340.
[52] Hennig, E. M., and Milani, T. L., 1993, ''The Tripod Support of the Foot. An Analysis of Pressure Distribution Under Static and Dynamic Loading,'' Z. Orthop. Ihre. Grenzgeb., **31**, pp. 279–284.
[53] Fung, Y. C., 1994, *A First Course in Continuum Mechanics*, Prentice Hall, Englewood Cliffs, NJ.
[54] Armstrong, D. G., Lavery, L. A, Harkless, L. B., and Van Houtum, W., 1997, ''Amputation and Reamputation of the Diabetic Foot,'' J. Am. Podiatr. Med. Assoc., **87**, pp. 255–259.
[55] Mueller, M. J., and Sinacore, D. R., 1994, ''Rehabilitation Factors Following Transmetatarsal Amputation,'' Phys. Ther., **74**, pp. 1027–1033.
[56] Sisto, S. A., 1998, ''An Overview of the Value of Information Resulting From Instrumented Gait Analysis for the Physical Therapist,'' *Gait Analysis in the Science of Rehabilitation*, T. T. Sowell, ed., Baltimore Rehabilitation Information and Technology Administrative Center, Baltimore, pp. 76–84.
[57] Netter, F. H., 1987, *The CIBA Collection of Medical Illustrations*, Ciba-Geigy, NJ.